

Quantum thermodynamics of holographic quenches and bounds on the growth of entanglement from the QNEC

Tanay Kibe, Ayan Mukhopadhyay and Pratik Roy*

*Center for Quantum Information Theory of Matter and Spacetime,
and Center for Strings, Gravitation and Cosmology, Department of Physics,
Indian Institute of Technology Madras, Chennai 600036, India*

(Dated: September 30, 2021)

The quantum null energy condition (QNEC) is a lower bound on the energy-momentum tensor in terms of the variation of the entanglement entropy of a sub-region along a null direction. To gain insights into quantum thermodynamics of many-body systems, we study if the QNEC restricts quenches driven by energy-momentum inflow from an infinite memoryless bath in two-dimensional holographic theories. We find that an increase in both entropy and temperature is necessary but not sufficient to not violate QNEC in quenches leading to transitions between rotating thermal states described by Banados-Teitelboim-Zanelli geometries. For an arbitrary initial state, we can determine the lower and upper bounds on the increase of temperature (entropy) that is necessary for a fixed increase in entropy (temperature). We also establish monotonic behavior of the non-saturation of the QNEC with time for allowed final states and analytically determine their asymptotic values – these should have new implications for the null shape variation of the relative entropy of the quenched state. Our study shows that the entanglement entropy always thermalizes in time $l/2$, where l is the length of the entangling region, with an exponent $3/2$. Furthermore, we are able to determine the rate of initial quadratic growth of entanglement analytically in terms of thermodynamic data for any l , and show that the QNEC bounds it from above and below. We also show that the slope of the asymptotic ballistic growth of entanglement for a semi-infinite interval is simply twice the difference of the entropy densities of the final and initial states.

INTRODUCTION

Quantum thermodynamics has established various instances where thermodynamics can be generalized even to finite-dimensional quantum systems interacting with a bath by accounting for entanglement and measures of accessible quantum information [1–7]. For instance, it has been shown that the one-shot work cost of creating a state with an epsilon-approximation is bounded by the epsilon dependent hypothesis-testing relative entropy between the state and the thermal equilibrium [3]. The latter also bounds the extractable work with the epsilon-approximation applied to the final excited state of a battery which performs the energy extraction. This discipline has found applications in understanding the limiting rates of (bio-)chemical reactions, and also in the study of quantum engines for novel technologies.

Although limited progress has been achieved in the applications of quantum thermodynamics to many-body systems, there have been independent developments of interest. One such example is the formulation of the Quantum Null Energy Condition (QNEC) [8] which sets a lower bound on the expectation value of null components of the energy-momentum tensor in terms of null variations of the entanglement entropy of a sub-region whose boundary contains the point of observation. QNEC has been proven in free field theories [9, 10], holographic quantum field theories [11] and also two-dimensional (2D) conformal field theories (CFTs) [12]. In a 2D CFT with central charge c , the strictest form of

QNEC is [11–13]

$$Q_{\pm} \equiv 2\pi \langle t_{\pm\pm} \rangle - S''_{ent} - \frac{6}{c} S'_{ent}{}^2 \geq 0, \quad (1)$$

where $t_{\pm\pm}$ are the two non-vanishing null components of the energy-momentum tensor, and the derivatives are obtained from the infinitesimal variations of the entanglement entropy S_{ent} of any interval ending at the point of observation under shifts along the $+$ (right) and $-$ (left) pointing null directions respectively. Recently it has been pointed out that QNEC is consistent with positivity conditions on variations of the relative entropy between a state and the vacuum under null shape deformations [14–16] (see also [17]). There is a measure of evidence that such positivity conditions also hold for sandwiched Renyi divergences, indicating existence of more general versions of QNEC [15, 16]. Therefore, a pertinent question is whether QNEC and its possible generalizations set criteria for physical realizations of processes (quench protocols) involving transitions between states that are stricter than those set by classical thermodynamics.

An unequivocal consequence of the laws of thermodynamics is that when any system with finite energy interacts with a memoryless infinitely large energy bath, its entropy can only increase monotonically. In holographic quantum field theories, this feature is reproduced via the monotonic growth of the area of the apparent and event horizons, and eventual thermalization when the system is subjected to quench protocols [18–21]. In this work, we consider quenches that lead to instantaneous transitions between rotating thermal states in 2D holographic

systems, and establish that the QNEC implies more than the mere rise of both the temperature and the thermodynamic entropy. For a fixed increase in the temperature (entropy), the increase in entropy (temperature) has to be bounded from both above and below so that the QNEC is unviolated in the large- c and strong coupling (implying sparse spectrum) limits, where a dual classical gravity description is valid. Furthermore, we establish that $\mathcal{Q}_+(t)$ and $\mathcal{Q}_-(t)$ for the semi-infinite interval are monotonic in time post quench.

In the present work, we extend previous results [22–29] on the growth and thermalization of the entanglement entropy in 2D CFTs in the context of holographic quenches describing transitions between arbitrary rotating thermal states. In particular, we establish that the entanglement entropy of an interval of length l always thermalizes in time $l/2$ with an exponent $3/2$, and grows linearly with time for a semi-infinite interval asymptotically with a slope that is twice the difference of the thermodynamic entropy densities between the final and initial states. We also determine analytically the coefficient of the initial post-quench quadratic growth of entanglement for arbitrary l . The criteria following from the validity of QNEC restricting possible transitions between rotating thermal states also set lower and upper bounds for the rates of growth of entanglement. Our results complement a similar upper bound discussed in [30].

HOLOGRAPHIC QUENCHES

A two-dimensional strongly coupled holographic CFT with a large central charge can be described by a three-dimensional Einstein gravity coupled to a few fields and with a negative cosmological constant [31]. The central charge of the dual CFT is $c = 3L/(2G)$ [32–34], where G is Newton’s gravitational constant and L is related to the cosmological constant Λ via $\Lambda = -1/L^2$.

Quenches leading to transitions between quantum equilibrium states (defined below) can be described by dual metrics of the form (see also [35])

$$ds^2 = 2drdt - \left(\frac{r^2}{L^2} - 2m(t, x)L^2 \right) dt^2 + 2j(t, x)L^2 dt dx + \frac{r^2}{L^2} dx^2 \quad (2)$$

in the ingoing Eddington-Finkelstein gauge. The coordinates t and x are shared by the dual field theory which lives at the boundary $r = \infty$ of the emergent radial direction. This geometry is supported by a bulk stress tensor T_{MN} whose non-vanishing components are

$$\begin{aligned} T_{tt} &= \frac{q(t, x)L^2}{r} + \frac{\partial_x p(t, x)L^4}{r^2} + \frac{p(t, x)j(t, x)L^6}{r^3}, \\ T_{tx} &= \frac{p(t, x)L^2}{r}. \end{aligned} \quad (3)$$

One can verify that T_{MN} of this form is traceless and locally conserved in the metric (2). The gravitational equations (with $\Lambda = -1/L^2$)

$$R_{MN} - \frac{1}{2}RG_{MN} - \frac{1}{L^2}G_{MN} = 8\pi G T_{MN} \quad (4)$$

are satisfied simply by requiring

$$\begin{aligned} \partial_t m(t, x) - \partial_x j(t, x) &= 8\pi G q(t, x), \\ \partial_t j(t, x) - \partial_x m(t, x) &= 8\pi G p(t, x). \end{aligned} \quad (5)$$

In absence of bulk matter, we therefore obtain

$$\begin{aligned} m(t, x) &= \mathcal{L}_+(x^+) + \mathcal{L}_-(x^-), \\ j(t, x) &= \mathcal{L}_+(x^+) - \mathcal{L}_-(x^-). \end{aligned} \quad (6)$$

with $x^\pm = t \pm x$, and \mathcal{L}_\pm being arbitrary chiral functions. These solutions are known as Banados geometries [36] and are related to the vacuum solution (for which $m(t, x) = j(t, x) = 0$) locally by a diffeomorphism that is non-vanishing at the boundary and is dual to a conformal transformation as will be shown later. See [37, 38] for detailed CFT interpretation. The dual CFT states have been called quantum equilibrium states since they saturate the QNEC inequalities (1) [39].

The gravitational constraints (5) imply that the metric (2) can describe instantaneous transitions between arbitrary quantum equilibrium states at $t = 0$ with the initial (i) and final (f) chiral functions being $\mathcal{L}_\pm^{i,f}$ so that

$$\begin{aligned} m &= \theta(-t)(\mathcal{L}_+^i(x^+) + \mathcal{L}_-^i(x^-)) + \theta(t)(\mathcal{L}_+^f(x^+) + \mathcal{L}_-^f(x^-)), \\ j &= \theta(-t)(\mathcal{L}_+^i(x^+) - \mathcal{L}_-^i(x^-)) + \theta(t)(\mathcal{L}_+^f(x^+) - \mathcal{L}_-^f(x^-)), \end{aligned}$$

if we set

$$\begin{aligned} 8\pi G q &= \delta(t)(\mathcal{L}_+^f(x) - \mathcal{L}_+^i(x) + \mathcal{L}_-^f(-x) - \mathcal{L}_-^i(-x)), \\ 8\pi G p &= \delta(t)(\mathcal{L}_+^f(x) - \mathcal{L}_+^i(x) - \mathcal{L}_-^f(-x) + \mathcal{L}_-^i(-x)). \end{aligned} \quad (8)$$

Holographic renormalization [33, 34] of the on-shell gravitational action for the metric (2) provides the expectation value of the energy-momentum tensor of the dual state (living in flat Minkowski metric):

$$\langle t_{\pm\pm} \rangle = \frac{c}{24\pi}(m(t, x) \pm j(t, x)), \quad \langle t_{+-} \rangle = 0. \quad (9)$$

The vanishing of $\langle t_{+-} \rangle$ implies tracelessness. The gravitational constraints (5) imply $\partial^\mu \langle t_{\mu\nu} \rangle = f_\nu$, where $f_\nu = -L(q(t, x), p(t, x))$ is the energy-momentum injection by the infinite bath into the CFT. In case of the instantaneous quench (7),

$$\langle t_{\pm\pm} \rangle = \frac{c}{12\pi} \left(\mathcal{L}_\pm^i(x^\pm)\theta(-t) + \mathcal{L}_\pm^f(x^\pm)\theta(t) \right). \quad (10)$$

We will focus on the case where the initial and final quantum equilibrium states are thermal states carrying momentum dual to rotating Banados-Teitelboim-Zanelli (BTZ) black branes [40, 41] so that $\mathcal{L}_\pm^{i,f} = \mu_\pm^{i,f^2}$. The

initial and final thermodynamic (Hawking) temperatures and the (Bekenstein-Hawking) thermodynamic entropy densities are given by

$$T_H^{i,f} = \frac{2}{\pi} \frac{\mu_+^{i,f} \mu_-^{i,f}}{\mu_+^{i,f} + \mu_-^{i,f}}, \quad s^{i,f} = \frac{c}{6} \left(\mu_+^{i,f} + \mu_-^{i,f} \right). \quad (11)$$

Also $\langle t_{\pm\pm} \rangle^{i,f} = (c/(12\pi)) \mu_{\pm}^{i,f2}$.

Here we have been agnostic about the matter content of the bulk theory as the form of the bulk energy-momentum tensor is simply necessitated by Einstein's equations. Our results therefore only rely on the assumption that instantaneous quenches can be realized as limiting processes.

THE CUT AND GLUE METHOD

For analytic computations, it is useful to notice that the geometry (2) describing an instantaneous transition (7) between two arbitrary Banados spacetimes at $t = 0$ can be *uniformized*, i.e. converted to the Poincaré patch metric, which corresponds to the vacuum with $m(t, x) = j(t, x) = 0$, with *separate* diffeomorphisms for $t < 0$ and $t > 0$. The full geometry can then be cut at $t = 0$ into two Poincaré patches and then glued back as described below. Our method is a substantial extension of the shift in the null coordinate employed in the context of homogeneous shocks in BTZ spacetimes [35, 42] to transitions between arbitrary inhomogeneous Banados spacetimes.

The uniformization map for a Banados solution (6) dual to a quantum equilibrium state can be defined in terms of new lightcone coordinates $X_b^\pm(x^\pm)$ that satisfy

$$\text{Sch}(X_b^\pm(x^\pm), x^\pm) = -2\mathcal{L}_\pm(x^\pm) \quad (12)$$

where Sch denotes the Schwarzian derivative. The uniformization map, which takes the metric (2) to the Poincaré patch metric with coordinates T , X and R is

$$\begin{aligned} T &= \frac{1}{2} \left(X_b^+(x^+) + X_b^-(x^-) \right. \\ &\quad \left. + \frac{X_b^{+'}(x^+) + X_b^{-'}(x^-) - 2\sqrt{X_b^{+'}(x^+)X_b^{-'}(x^-)}}{\frac{r}{L^2} - \frac{X_b^{+''}(x^+)}{2X_b^{+'}(x^+)} - \frac{X_b^{-''}(x^-)}{2X_b^{-'}(x^-)}} \right), \\ X &= \frac{1}{2} \left(X_b^+(x^+) - X_b^-(x^-) + \frac{X_b^{+'}(x^+) - X_b^{-'}(x^-)}{\frac{r}{L^2} - \frac{X_b^{+''}(x^+)}{2X_b^{+'}(x^+)} - \frac{X_b^{-''}(x^-)}{2X_b^{-'}(x^-)}} \right), \\ R &= L^2 \frac{\frac{r}{L^2} - \frac{X_b^{+''}(x^+)}{2X_b^{+'}(x^+)} - \frac{X_b^{-''}(x^-)}{2X_b^{-'}(x^-)}}{\sqrt{X_b^{+'}(x^+)X_b^{-'}(x^-)}}. \end{aligned} \quad (13)$$

It is easy to see that at the boundary $r = \infty$, $X^\pm = T \pm X$ reduces to $X_b^\pm(x^\pm)$ respectively – so the boundary lightcones are reparametrized following (12). The boundary

metric, which is identified with the physical metric on which the CFT lives, still remains the flat Minkowski space. The uniformization map transforms $\langle t_{\pm\pm} \rangle$ of the dual quantum equilibrium state to zero in agreement with the conformal anomaly of the dual CFT, provided the central charge is indeed $c = 3L/(2G)$. For BTZ solutions, we choose

$$X_b^\pm(x^\pm) = L \exp(2\mu_\pm x^\pm). \quad (14)$$

The uniformization map is valid only outside the outer horizon $r_{out} = L^2(\mu^+ + \mu^-)$ with the latter mapping to the Poincaré horizon $R = 0$. Note that (12) determines $X_b^\pm(x^\pm)$ only up to an overall $SL(2, R)$ (fractional linear) transformation, which accounts for the local $SL(2, R) \times SL(2, R)$ isometries of Banados metrics. It is convenient to fix to choose X_b^\pm such that ∞ is a fixed point, $X_b^\pm(-\infty) = 0$ and $X_b^\pm(0) = L$.

The cut and glue method is essentially then employing two different uniformization maps ($T^{i,f}(t, x, r)$, $X^{i,f}(t, x, r)$, $R^{i,f}(t, x, r)$) before and after the quench, with $X_b^{\pm i}(x^\pm)$ determined by $\mathcal{L}_\pm^i(x^\pm)$ for $t < 0$ and $X_b^{\pm f}(x^\pm)$ determined by $\mathcal{L}_\pm^f(x^\pm)$ for $t > 0$ respectively. These maps result in two hypersurfaces, which are simply the respective images of the hypersurface $t = 0$:

$$\Sigma^{i,f} = (T^{i,f}(0, x, r), X^{i,f}(0, x, r), R^{i,f}(0, x, r)). \quad (15)$$

These two hypersurfaces should be glued by identifying the points on each one with same *physical* coordinate values x and r . Note that the Israel junction conditions are already implied by (8) which determine the bulk energy-momentum tensor (3).

ENTANGLEMENT GROWTH

The entanglement entropy of a spacelike interval with end points $p_1 = (x_1, t_1)$ and $p_2 = (x_2, t_2)$ in any arbitrary state of the holographic CFT can be obtained from the proper length L_{geo} of the geodesic in the dual bulk geometry which is anchored to the points p_1 and p_2 at the regulated boundary $r = L^2/\epsilon$, and is given by [43, 44]

$$S_{ent} = \frac{c}{6} \frac{L_{\text{geo}}}{L}. \quad (16)$$

ϵ^{-1} is interpreted as an ultraviolet energy cutoff in the dual theory. Employing the uniformization map given by (13) and (14), the geodesic length can be readily computed in the Poincaré patch. Note the points at the (13) boundary in the Poincaré patch are given by $X_{1,2}^\pm = X_b^\pm(x_{1,2}^\pm)$ in terms of the boundary lightcone coordinates. A simple computation yields

$$S_{ent} = \frac{c}{6} \ln \left(\frac{\sinh(\mu_+ l) \sinh(\mu_- l)}{\mu_+ \mu_- l^2} \right) + \frac{c}{3} \ln \left(\frac{l}{\epsilon} \right), \quad (17)$$

where the last term is the vacuum contribution that depends on the ultraviolet regulator (see [22, 45, 46]). A similar computation (see also [47]) yields the entanglement entropy in an arbitrary Banados geometry and establishes the saturation of the QNEC (1), i.e. \mathcal{Q}_\pm vanishes in dual quantum equilibrium states [39].

In order to compute the entanglement for a geometry describing an instantaneous quench (7), we can readily employ the cut and glue method. Before the quench, the geodesic is located entirely in the initial Poincaré patch described by the first uniformization map for $t < 0$, but after the quench the geodesic anchored to the boundary of the final Poincaré patch goes back in time and intersects the gluing hypersurface Σ^f , given by (15), at two points until a limiting thermalization time where the two intersection points merge. Afterwards, the geodesic lies entirely in the final Poincaré patch. The intersection points (between quench and until thermalization time) can be readily obtained by substituting Σ^f described by (15) into the two geodesic equations (fixed by the boundary points), and solving for the physical coordinates (x_*, r_*) that parametrize Σ^f . The semi-circular geodesic in the final Poincaré patch is thus cut into two arcs ending at the boundary points. Substituting the parameters (x_*, r_*) for the two intersection points in the expression for Σ^i in (15), we obtain their images in the initial Poincaré patch where the final semi-circular arc is completed. The combined length of the three geodesic arcs lead to the entanglement entropy. Similarly, one can compute its variation under null deformations of any of the endpoints. For more details see Supplementary Material.

Our explicit computations confirm that the entanglement entropy has three stages of evolution [24–26] for an arbitrary transition between two BTZ spacetimes. In the first stage, the entanglement entropy of an interval of length l grows quadratically from its pre-quench values as $\sim D_s t^2$ with

$$D_s = \frac{c}{6} \left(\Delta m + 2 \left(\mu_+^f \coth(\mu_+^f l) - \mu_+^i \coth(\mu_+^i l) \right) \right. \\ \left. \left(\mu_-^f \coth(\mu_-^f l) - \mu_-^i \coth(\mu_-^i l) \right) \right), \quad (18)$$

where $\Delta m = \mu_+^{f2} + \mu_-^{f2} - \mu_+^{i2} - \mu_-^{i2}$. The above reproduces the known result for the vacuum to thermal non-rotating BTZ transition [24, 26]. In the intermediate regime, the entanglement grows quasi-linearly. For a semi-infinite interval, the asymptotic growth is exactly linear, i.e. $S_{ent} = v_s t$ with

$$v_s = 2(s^f - s^i) \quad (19)$$

where $s^{i,f}$ are the initial (final) entropy densities given by (11). This is consistent with the *tsunami hypothesis* [25, 29] (see also [48–50]) that the entanglement *spreads*

with a tsunami velocity, which is the speed of light in 2D CFTs [23, 29], from both ends of the interval so that the sub-intervals of total length $2t$ should have been completely entangled with the rest of the quenched system. If an interval of large length can be approximated by a thermal density matrix (see [23, 51–53]), then the result follows because the change in the entanglement at late time should be the product of the length $2t$ times the difference in the thermodynamic entropy densities between final and initial states (see [54, 55] for other contexts).

The entanglement entropy thermalizes at time $t = l/2$ in consistency with the interpretation of the tsunami velocity being the speed of light [23–26, 29]. The final intersection point of the geodesic with the gluing surface Σ^f at $t = l/2$ is given by the point parametrized by

$$r_* = L^2(\mu_+^f \coth(\mu_+^f l) + \mu_-^f \coth(\mu_-^f l)), \quad x_* = l/2, \quad (20)$$

which lies outside the outer horizon. One can readily obtain that the entanglement entropy saturates as $S_{ent}^f - S_{ent}^i(t) \sim (l/2 - t)^{3/2}$ as the time approaches $l/2$. The exponent $3/2$ was earlier noticed for the vacuum to non-rotating BTZ transition [24–26]. It will be interesting to see how to reproduce these results via tensor network approaches building on [56].

THE QNEC CRITERION

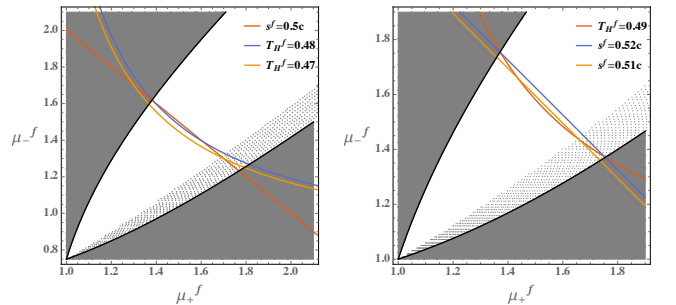


FIG. 1. The possible final states for $\mu_+^i = 1, \mu_-^i = 0.75$ (left) and $\mu_\pm^i = 1$ (right) are shown in white. The black lines are given by the inequality (21) implying $\mathcal{Q}_\pm(t = 0^+) \geq 0$ and grey region is disallowed by examining \mathcal{Q}_- for $t > 0$. For a fixed final entropy density (temperature), the final temperature (entropy) is bounded from above and below.

While applying QNEC inequalities (1) for $t > 0$ in the case of instantaneous quenches leading to transitions between rotating thermal states, we find that the inequality (1) is the strictest when we consider the semi-infinite interval (see Supplementary Material for dependence of \mathcal{Q}_\pm on l). Translation symmetry further implies that it is sufficient to consider the interval $x \geq 0$ with \mathcal{Q}_+ (\mathcal{Q}_-) involving null variations of the spatial origin towards right (left) respectively. Applying the cut and glue method for

the semi-infinite interval, we see that demanding $\mathcal{Q}_\pm \geq 0$ at $t = 0$ implies (with $\Delta = 2(\mu_+^f - \mu_+^i)(2\mu_+^f + \mu_+^i)$):

$$\frac{1}{3} \left(\sqrt{\Delta + 3\mu_-^i(3\mu_-^i + 2\mu_+^i - 2\mu_+^f)} + \mu_+^f - \mu_+^i \right) \leq \mu_-^f \leq \sqrt{\Delta + \mu_-^i(\mu_-^i + 2\mu_+^f - 2\mu_+^i)} - \mu_+^f + \mu_+^i. \quad (21)$$

For initial vacuum state ($\mu_\pm^i = 0$), the above inequalities simply impose that $\mu_\pm^f = \mu_\pm^i$, i.e. the final state should have zero momentum. One can analytically show that for the latter case $\mathcal{Q}_\pm = 0$ for all time in the case of the semi-infinite interval (see Supplementary Material). It is quite interesting that although the thermalization of the the entanglement occurs at the tsunami speed (of light), the QNEC saturation perpetuates after the quench.

When the initial state is not the vacuum, the inequality (21) implies that $\mu_\pm^f \geq \mu_\pm^i$, and therefore $T_H^f > T_H^i$ and $s^f > s^i$, i.e. both the Hawking temperature and thermodynamic entropy density must increase unless $\mu_\pm^f = \mu_\pm^i$ (no quench). With $\mu_+^i = 1$, $\mu_-^i = 0.75$ (and $\mu_\pm^i = 1$), as for instance, the final states which satisfy (21) lie within the bold black lines in the left (and right) of Fig. 1. It is easy to see that (21) always sets stricter criteria than mere increase of temperature and entropy densities.

When the upper (lower) end of the inequality (21) is satisfied, \mathcal{Q}_+ (\mathcal{Q}_-) vanishes at $t = 0$ for the semi-infinite interval. For $t > 0$, although $\mathcal{Q}_+ > 0$ is always satisfied when (21) holds, $\mathcal{Q}_- \geq 0$ is violated for $t > t_c$ (with t_c depending on initial and final states) unless the lower bound on μ_-^f set by (21) is pushed above, depicted by the upper boundaries of the dotted regions in Fig. 1 (see Supplementary Material for more details). The final allowed region, shown in white in Fig. 1, implies lower and upper bounds on the increase in temperature (entropy density) for a fixed increase in entropy density (temperature). Furthermore, we find that as $t \rightarrow \infty$,

$$\mathcal{Q}_- \rightarrow 0, \quad \mathcal{Q}_+ \rightarrow (s^f - s^i)(\mu_+^f - \mu_-^f + \mu_+^i + \mu_-^i) > 0. \quad (22)$$

(The inequality above follows from (21).) Crucially, for the allowed transitions in which QNEC is unviolated, $\mathcal{Q}_+(t)$ and $\mathcal{Q}_-(t)$ for the semi-infinite interval are also monotonically increasing and decreasing functions of time respectively for $t > 0$. Its implications for the null shape variation of the relative entropy of the quenched state with respect to the vacuum/initial state should be understood following [15, 57].

The existence of upper and lower bounds on Δs , the increase in entropy density, for a fixed final temperature and an initial state, readily bounds the speed of the asymptotic ballistic entanglement growth (19) for the semi-infinite interval from both above and below. Furthermore, the coefficient of the initial quadratic growth (18) is similarly bounded from above and below for any l , and both of these bounds increase monotonically with l (plots in the Supplementary Material).

DISCUSSION

We have developed a method for studying instantaneous quenches between arbitrary quantum equilibrium states generated via energy-momentum inflow from an infinitely large bath. We have also established that QNEC sets criteria stricter than the mere increase of both temperature and entropy density, especially for transitions between rotating thermal states, implying bounds on the rate of growth of entanglement. We have checked that transitions from thermal states to inhomogeneous quantum equilibrium states are disallowed – the entanglement entropy decreases and QNEC is violated as the chirally propagating finite-width excitations leave the entangling interval [58]. However transitions where inhomogeneous excitations are deleted and replaced by a homogeneous energy density could be allowed. A study of such possibilities would allow us to make contact with the Landauer principle [59–61]. We wish to do a more general study of transitions between quantum equilibrium states in the future. Furthermore, it will be interesting to construct quantum engines by exploiting suitable bulk matter.

It is a pleasure to thank Shira Chapman, Christian Ecker, Daniel Grumiller, Arul Lakshminarayan, Prabha Mandayam, Marios Petropoulos, Giuseppe Policastro and Suhail Ahmad Rather for helpful discussions. We also thank Souvik Banerjee for collaboration during early stages of this work, and Avik Banerjee and Nehal Mittal for collaboration on further investigations to appear in a future publication. The research of TK is supported by the Prime Minister's Research Fellowship (PMRF). AM acknowledges the support of the Ramanujan Fellowship of the Science and Engineering Board of the Department of Science and Technology of India, the new faculty seed grant of IIT Madras and the additional support from the Institute of Eminence scheme of IIT Madras funded by the Ministry of Education of India.

SUPPLEMENTARY MATERIAL

Computation of the entanglement entropy and QNEC by the cut and glue method

Let $x_{1,2}^\pm$ denote the lightcone coordinates of the endpoints of the entangling interval whose entanglement entropy is of interest. In the dual Banados spacetime we place these points at the boundary $r = \infty$. When we map this spacetime to the Poincaré patch metric given by (2) with $m(t, x) = j(t, x) = 0$ via the uniformization map (13), the endpoints get mapped to $(X_b^+(x_1^+), X_b^-(x_1^-))$ and $(X_b^+(x_2^+), X_b^-(x_2^-))$ at the boundary $R = \infty$ as mentioned in the text. These endpoints are denoted as p_1 and p_2 in Fig. 2. In what follows, it is useful to redefine the Poincaré patch radial coordinate as $Z = L^2/R$ so that the boundary is at $Z = 0$. Explicitly, the endpoints

of the entangling interval at the boundary are at

$$\begin{aligned} T_1 &= \frac{1}{2}(X_b^+(x_1^+) + X_b^-(x_1^-)), X_1 = \frac{1}{2}(X_b^+(x_1^+) - X_b^-(x_1^-)), \\ Z_1 &= 0, \\ T_2 &= \frac{1}{2}(X_b^+(x_2^+) + X_b^-(x_2^-)), X_2 = \frac{1}{2}(X_b^+(x_2^+) - X_b^-(x_2^-)), \\ Z_2 &= 0. \end{aligned} \quad (23)$$

The equations for the geodesic in the Poincaré patch metric connecting any two endpoints (T_1, X_1, Z_1) and (T_2, X_2, Z_2) are given by the two equations

$$\begin{aligned} Z + T - \frac{T_1 + T_2}{2} - \frac{T_2 - T_1}{X_2 - X_1} \left(X - \frac{X_1 + X_2}{2} \right) &= 0, \\ \frac{Z^2}{(X_2 - X_1)^2 - (T_2 - T_1)^2} - \frac{(2X - X_1 - X_2)^2}{4(X_2 - X_1)^2} &= \frac{1}{4}. \end{aligned} \quad (24)$$

As shown in Fig. 2, when the endpoints lie in the post-quench geometry, the above geodesic is cut into three segments by the cut and glue prescription described in the main text. The intersection points of the geodesic and the glueing hypersurface Σ^f parametrized by the physical coordinates x and r can be found by substituting (23) and the equation for Σ^f in (15) into the above two equations (24) for the geodesic, and solving for x and r . We obtain at most two pairs of solutions giving the two intersection points $q_1(x_1^*, r_1^*)$ and $q_2(x_2^*, r_2^*)$ shown in Fig. 2. The image of the intersection points on Σ^i is obtained simply by substituting the values of $x_{1,2}^*$ and $r_{1,2}^*$ into

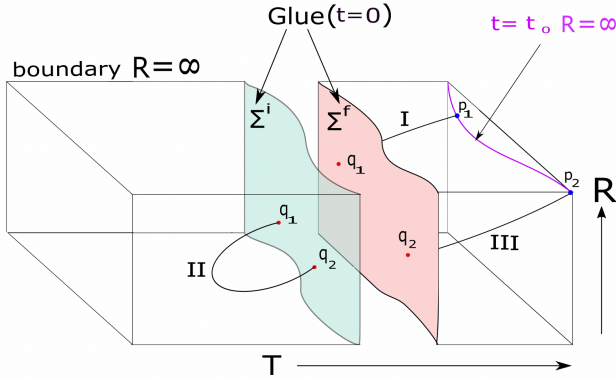


FIG. 2. Schematic representation of the cut and glue method to compute the entanglement entropy – the left and right halves represent the separate Poincaré patches to which the pre-quench and post-quench Banados spacetimes map to. The glueing hypersurfaces $\Sigma^{i,f}$ are the images of $t = 0$ in the respective geometries and are given by (15). Points on these hypersurfaces carrying the same physical coordinate labels x and r should be identified. The geodesic ending at the boundary is cut into three arcs by these hypersurfaces.

the equation in (15) describing Σ^i . The geodesic with these endpoints in the pre-quench Poincaré patch is then completed by the arc following the equations (24) with endpoints chosen to be these intersection points (see Fig. 2). To compute the length of the arcs we simply need the endpoints explicitly and employ the invariant distance formula [62].

For BTZ geometries, the explicit form of X_b^\pm given by (14) allows for explicit analytic solutions of the intersection points at early time and near thermalization time ($l/2$) generically, and for all times when the final state is non-rotating. When the boundary interval is at $t = l/2$, the two intersection points merge into one as given by (20) – the geodesic intersects Σ^f tangentially at this point and lies entirely in the post-quench Poincaré patch otherwise. For $t > l/2$, the geodesic does not intersect the glueing hypersurface. When $t \sim 0$, the intersection points can be computed in power series in t .

It is obvious that the above computation can be repeated after displacing one of the two boundary endpoints to obtain \mathcal{Q}_\pm .

We should be able to use this method also to study retarded correlation functions in quenched geometries following [63] – in this case one needs to analytically continue the bulk fields across the glueing surface.

Explicit results for S_{ent} and \mathcal{Q}_\pm for quenches leading to a non-rotating BTZ state

Since the intersection points $q_{1,2}$ can be computed for all time t for a final non-rotating BTZ state, we can obtain the time-dependent entanglement entropy for any quench from an arbitrary rotating BTZ (with parameters μ_\pm^i) to final non-rotating BTZ state (with $\mu_\pm^f = \mu$). The final expression is however very cumbersome and simplifies only in the limit when the entangling region has large length l . Explicitly,

$$\begin{aligned} S_{ent} &= \frac{c}{6} \ln \left(\frac{4\mu^2 \cosh^2(2\mu t) - (\mu_+^i - \mu_-^i)^2 \sinh^2(2\mu t)}{4\mu^2 \cosh(2\mu t) \frac{\mu_+^i + \mu_-^i}{\mu}} \right) \\ &+ \frac{c}{6} \ln \left(\frac{\sinh(\mu_+^i l) \sinh(\mu_-^i l)}{\epsilon^2 \mu_+^i \mu_-^i} \right) + \dots, \end{aligned} \quad (25)$$

with \dots denoting terms which vanish as $l \rightarrow \infty$. The above agrees with the rates of entanglement growth given by (18) (with $l \rightarrow \infty$) and also with (19) for $\mu_\pm^f = \mu$. It also reproduces the known result [24, 26] for vacuum to non-rotating BTZ transition.

Similarly one can obtain $\mathcal{Q}_\pm(t)$ analytically for any entangling length l for all time explicitly when the final state is thermal and non-rotating. Note that unlike the entanglement entropy, $\mathcal{Q}_\pm(t)$ is discontinuous at $t = 0$ due to the discontinuity of the derivatives of S_{ent} at the quenching time. Explicitly for $t > 0$ and $l \rightarrow \infty$ (i.e. for

the semi-infinite interval $x \geq 0$),

$$\begin{aligned} \mathcal{Q}_+ &= \frac{c}{24} \frac{e^{4\mu t}(\mu_+^i + \mu_-^i) \text{sech}^2(2\mu t)}{2\mu - (\mu_+^i - \mu_-^i) \tanh(2\mu t)} \left(2\mu(2\mu + \mu_-^i - 3\mu_+^i) \right. \\ &\quad \left. + (\mu_+^i - \mu_-^i)(2\mu + \mu_+^i + \mu_-^i) \tanh(2\mu t) \right), \\ \mathcal{Q}_- &= \frac{c}{24} \frac{e^{-4\mu t}(\mu_+^i + \mu_-^i) \text{sech}^2(2\mu t)}{2\mu - (\mu_+^i - \mu_-^i) \tanh(2\mu t)} \left(2\mu(2\mu + \mu_+^i - 3\mu_-^i) \right. \\ &\quad \left. + (\mu_+^i - \mu_-^i)(2\mu + \mu_+^i + \mu_-^i) \tanh(2\mu t) \right). \end{aligned} \quad (26)$$

Requiring \mathcal{Q}_\pm to be non-negative at $t = 0$ is equivalent to (21) for $\mu_-^f = \mu_+^f = \mu$. When the initial state is the vacuum, \mathcal{Q}_\pm vanishes for all times for the semi-infinite interval as evident from (26), and as claimed in the main text. For an arbitrary initial state, (26) implies that \mathcal{Q}_+ plateaus at $t \rightarrow \infty$ to a finite value while \mathcal{Q}_- vanishes in agreement with (22).

For finite l and arbitrary initial and final states, \mathcal{Q}_+ diverges as $(l/2 - t)^{-1/2}$ and \mathcal{Q}_- vanishes as $t \rightarrow l/2$; and both vanish for $t > l/2$ due to thermalization of the entanglement entropy. The coefficient $-1/2$ of the divergence of \mathcal{Q}_+ is simply a consequence of the saturation exponent $3/2$ of the entanglement entropy at $t = l/2$ mentioned earlier (and is the result of the double derivative, S'' , in QNEC). Plots of \mathcal{Q}_\pm for a representative transition to a final thermal non-rotating state are shown in Fig. 3 as a function of time ($t > 0$) for different values of l of the entangling interval $0 \leq x \leq l$. It is clear from the plots that the QNEC inequality (1) gets stricter uniformly for $t > 0$ as $l \rightarrow \infty$. This also holds for arbitrary transitions. We reproduce features of the numerical results for vacuum to non-rotating BTZ transitions for finite l reported in [39].

Computing \mathcal{Q}_\pm for the semi-infinite interval and determining allowed quenches

For arbitrary quenches between rotating thermal states, the QNEC inequality is the strictest for the semi-infinite interval as described above. For a generic instantaneous quench between thermal rotating states, we can compute \mathcal{Q}_\pm for this semi-infinite interval analytically just after the quench i.e. when $t > 0$ and is small, and also when t is large, as in both cases we can obtain analytic expressions for the intersection points between the geodesic and the glueing hypersurface. At $t = 0$, \mathcal{Q}_\pm jumps discontinuously from zero to the finite values:

$$\mathcal{Q}_+(t = 0^+) = \frac{c}{24} (3(\mu_+^{f2} - \mu_+^{i2}) + (\mu_-^f - \mu_-^i)(2\mu_+^i - 2\mu_+^f - \mu_-^f - \mu_-^i)), \quad (27)$$

and

$$\mathcal{Q}_-(t = 0^+) = \frac{c}{24} (3(\mu_-^{f2} - \mu_-^{i2}) + (\mu_+^f - \mu_+^i)(2\mu_-^i - 2\mu_-^f - \mu_+^f - \mu_+^i)) \quad (28)$$

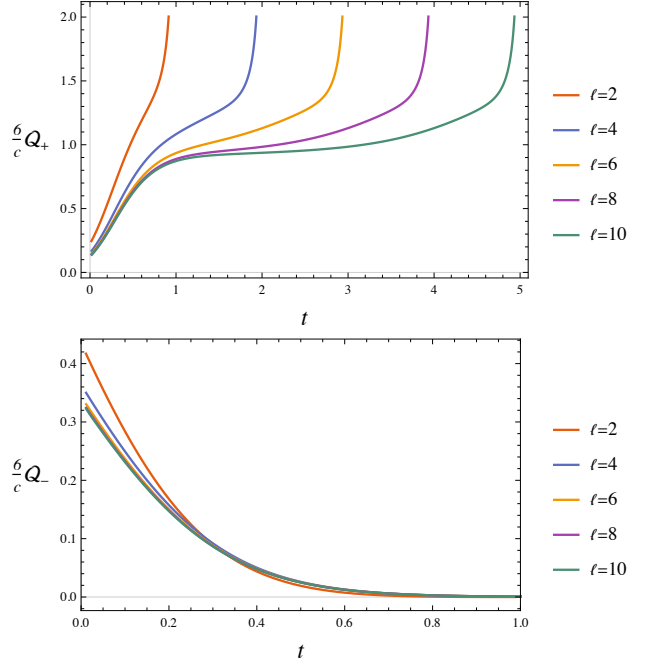


FIG. 3. \mathcal{Q}_+ (top) is plotted for $0 < t < l/2$ and \mathcal{Q}_- (bottom) is plotted for $0 < t < \min(1, l/2)$ for various lengths l of the entangling interval and the instantaneous quench from $\mu_+^i = 0.5, \mu_-^i = 0.2$ to the non-rotating final state with $\mu_\pm^f = 1$. It is clear that the strictest inequality is imposed in the limit $l \rightarrow \infty$. Note \mathcal{Q}_\pm vanishes for $t < 0$ and $t > l/2$.

respectively. These are in agreement with the result for $\mathcal{Q}_\pm(t)$ given by (26) when evaluated at $t = 0$ and with $\mu_\pm^f = \mu$. Note that $\mathcal{Q}_\pm(t = 0^+)$ are related by simultaneous interchanges of μ_+^i with μ_-^i and μ_+^f with μ_-^f , i.e. the left and right moving temperatures. (This is not true for $t > 0$.) Requiring $\mathcal{Q}_\pm(t = 0^+) \geq 0$ and using (27) and (28) we obtain the inequalities given in (21). We will call the upper bound on μ_-^f given by (21) as μ_-^u and the lower bound as μ_-^l . Both μ_-^u and μ_-^l are determined by μ_\pm^i and μ_\pm^f . We study $\mathcal{Q}_\pm(t)$ by numerical determinations of the intersection points at intermediate times for generic transitions.

$\mathcal{Q}_+(t)$ increases monotonically in time if $\mathcal{Q}_+(t = 0^+) > 0$ and saturates to the value given by (22) as $t \rightarrow \infty$ (see Fig. 4 for plots). It is therefore sufficient to check if $\mathcal{Q}_+(t = 0^+) > 0$ to satisfy $\mathcal{Q}_+(t) > 0$ for $t > 0$. This is guaranteed if $\mu_-^l < \mu_-^f < \mu_-^u$ as illustrated in Fig. 4.

$\mathcal{Q}_-(t)$ can be a non-monotonic function even if $\mathcal{Q}_-(t = 0^+) > 0$. However, there exists μ_-^{lr} such that $\mu_-^u > \mu_-^{lr} > \mu_-^l$ for which $\mathcal{Q}_-(t)$ is positive for all $t > 0$ and is also a monotonically decreasing function if $\mu_-^{lr} < \mu_-^f$. See Fig. 5 for an illustration.

To find the final allowed quenches, where both $\mathcal{Q}_\pm(t)$ are non-negative for $t \geq 0$, it is therefore sufficient to restrict μ_-^f within the upper and lower bounds set by (21) for given μ_\pm^i , and then scan upwards by increasing

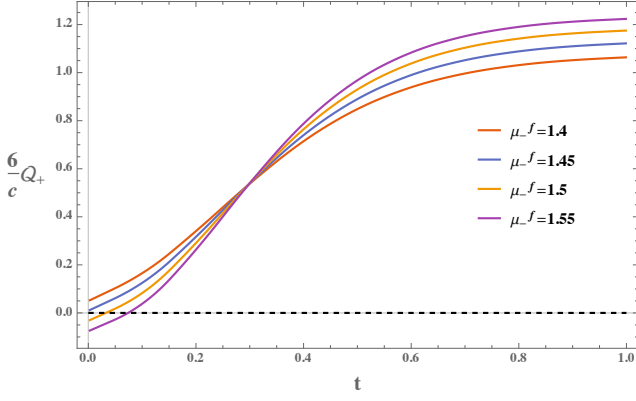


FIG. 4. Q_+ as a function of time is plotted above for $\mu_{\pm}^i = 1$ and $\mu_+^f = 1.2$, and various values of μ_i^f . Note that (21) implies $\mu_-^l \approx 1.08$ and $\mu_-^u \approx 1.46$. We see that Q_+ increases monotonically and saturates to the value given by Eq. 22 of the main text as $t \rightarrow \infty$ if $\mu_-^l < \mu_-^f < \mu_-^u$.

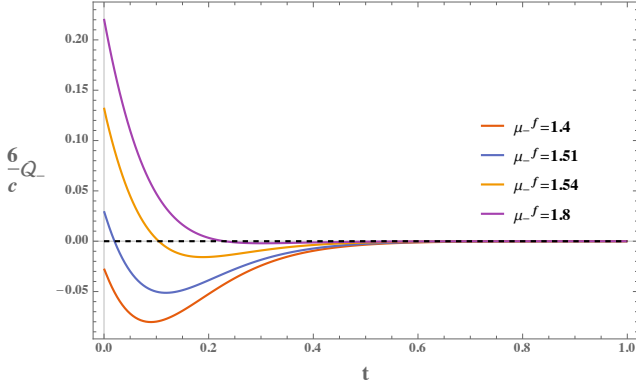


FIG. 5. Q_- as a function of time is plotted above for $\mu_{\pm}^i = 1$ and $\mu_+^f = 2$, and various values of μ_i^f . According to (21), $\mu_-^l \approx 1.54$ and $\mu_-^u \approx 2.61$. We see that after a finite time Q_- becomes negative even if $Q_-(t=0^+) > 0$, i.e. $\mu_-^f > \mu_-^l$. However for $\mu_-^{lr} < \mu_-^f < \mu_-^u$, $Q_-(t) > 0$ for $t > 0$ and is also a monotonically decreasing function which vanishes at late time. Here $\mu_-^{lr} \approx 1.6$.

μ_-^f from the lower end μ_-^l for fixed μ_+^f until we find μ_-^{lr} such that $Q_-(t)$ stays positive for all $t > 0$. This gives us the allowed final states $\mu_-^{lr}(\mu_+^f) \leq \mu_-^f \leq \mu_-^u(\mu_+^f)$ for a given μ_{\pm}^i (the white regions shown in Fig. 1). In this allowed region, Q_+ and Q_- are monotonically increasing and decreasing functions of time respectively (it is easy to check analytically via (26) when the final non-rotating state is allowed).

Lower and upper bounds on D_s

One can convert the restriction $\mu_-^{lr}(\mu_+^f) \leq \mu_-^f \leq \mu_-^u(\mu_+^f)$ set by the QNEC for a fixed initial μ_{\pm}^i to a lower and upper bound for the entropy density (temperature)

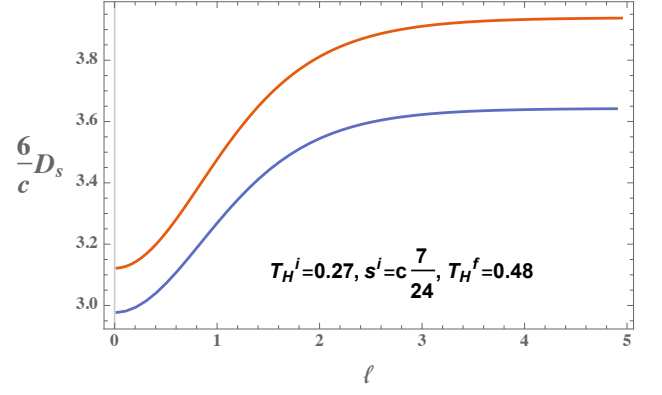


FIG. 6. The upper and lower bounds on D_s for a fixed initial state and a final temperature are plotted above as a function of l in red and blue respectively. Both of these bounds increase with l monotonically.

for a fixed final temperature (entropy density) via (11). Substituting these in (18), one readily obtains a lower and an upper bound on D_s for a fixed initial temperature and entropy density, and a fixed final temperature (as shown in Fig. 6) or for a fixed final entropy density. Both the lower and upper bounds increase monotonically with l .

-
- * ayan@physics.iitm.ac.in, tanayk@smail.iitm.ac.in,
pratik@physics.iitm.ac.in
- [1] Fernando G. S. L. Brandão and Gilad Gour, “Reversible framework for quantum resource theories,” *Phys. Rev. Lett.* **115**, 070503 (2015).
 - [2] Yelena Guryanova, Sandu Popescu, Anthony J. Short, Ralph Silva, and Paul Skrzypczyk, “Thermodynamics of quantum systems with multiple conserved quantities,” *Nature Communications* **7** (2016), 10.1038/ncomms12049.
 - [3] Nicole Yunger Halpern and Joseph M. Renes, “Beyond heat baths: Generalized resource theories for small-scale thermodynamics,” *Phys. Rev. E* **93**, 022126 (2016).
 - [4] Nicole Yunger Halpern, Philippe Faist, Jonathan Oppenheim, and Andreas Winter, “Microcanonical and resource-theoretic derivations of the thermal state of a quantum system with noncommuting charges,” *Nature Communications* **7** (2016), 10.1038/ncomms12051.
 - [5] John Goold, Marcus Huber, Arnau Riera, Lidia del Rio, and Paul Skrzypczyk, “The role of quantum information in thermodynamics—a topical review,” *Journal of Physics A: Mathematical and Theoretical* **49**, 143001 (2016).
 - [6] Gilad Gour, David Jennings, Francesco Buscemi, Runyao Duan, and Iman Marvian, “Quantum majorization and a complete set of entropic conditions for quantum thermodynamics,” *Nature Communications* **9** (2018), 10.1038/s41467-018-06261-7.
 - [7] Eric Chitambar and Gilad Gour, “Quantum resource theories,” *Rev. Mod. Phys.* **91**, 025001 (2019).

- [8] Raphael Bousso, Zachary Fisher, Stefan Leichenauer, and Aron C. Wall, “Quantum focusing conjecture,” *Physical Review D* **93** (2016), 10.1103/physrevd.93.064044.
- [9] Raphael Bousso, Zachary Fisher, Jason Koeller, Stefan Leichenauer, and Aron C. Wall, “Proof of the quantum null energy condition,” *Physical Review D* **93** (2016), 10.1103/physrevd.93.024017.
- [10] Taha A. Malik and Rafael Lopez-Mobilia, “Proof of the quantum null energy condition for free fermionic field theories,” *Phys. Rev. D* **101**, 066028 (2020), arXiv:1910.07594 [hep-th].
- [11] Jason Koeller and Stefan Leichenauer, “Holographic proof of the quantum null energy condition,” *Physical Review D* **94** (2016), 10.1103/physrevd.94.024026.
- [12] Srivatsan Balakrishnan, Thomas Faulkner, Zuhair U. Khandker, and Huajia Wang, “A General Proof of the Quantum Null Energy Condition,” *JHEP* **09**, 020 (2019), arXiv:1706.09432 [hep-th].
- [13] Aron C. Wall, “Testing the Generalized Second Law in 1+1 dimensional Conformal Vacua: An Argument for the Causal Horizon,” *Phys. Rev. D* **85**, 024015 (2012), arXiv:1105.3520 [gr-qc].
- [14] Stefan Leichenauer, Adam Levine, and Arvin Shahbazi-Moghaddam, “Energy density from second shape variations of the von Neumann entropy,” *Phys. Rev. D* **98**, 086013 (2018), arXiv:1802.02584 [hep-th].
- [15] Nima Lashkari, “Constraining Quantum Fields using Modular Theory,” *JHEP* **01**, 059 (2019), arXiv:1810.09306 [hep-th].
- [16] Mudassir Moosa, Pratik Rath, and Vincent Paul Su, “A Rényi quantum null energy condition: proof for free field theories,” *JHEP* **01**, 064 (2021), arXiv:2007.15025 [hep-th].
- [17] Fikret Ceyhan and Thomas Faulkner, “Recovering the QNEC from the ANEC,” *Commun. Math. Phys.* **377**, 999–1045 (2020), arXiv:1812.04683 [hep-th].
- [18] James M. Bardeen, B. Carter, and S. W. Hawking, “The Four laws of black hole mechanics,” *Commun. Math. Phys.* **31**, 161–170 (1973).
- [19] V. Balasubramanian, A. Bernamonti, J. de Boer, N. Copland, B. Craps, B. Keski-Vakkuri, B. Muller, A. Schafer, M. Shigemori, and W. Staessens, “Thermalization of Strongly Coupled Field Theories,” *Phys. Rev. Lett.* **106**, 191601 (2011), arXiv:1012.4753 [hep-th].
- [20] Veronika E. Hubeny and Mukund Rangamani, “A Holographic view on physics out of equilibrium,” *Adv. High Energy Phys.* **2010**, 297916 (2010), arXiv:1006.3675 [hep-th].
- [21] Paul M. Chesler and Laurence G. Yaffe, “Numerical solution of gravitational dynamics in asymptotically anti-de Sitter spacetimes,” *JHEP* **07**, 086 (2014), arXiv:1309.1439 [hep-th].
- [22] Pasquale Calabrese and John L. Cardy, “Entanglement entropy and quantum field theory,” *J. Stat. Mech.* **0406**, P06002 (2004), arXiv:hep-th/0405152.
- [23] Pasquale Calabrese and John Cardy, “Entanglement entropy and conformal field theory,” *J. Phys. A* **42**, 504005 (2009), arXiv:0905.4013 [cond-mat.stat-mech].
- [24] Veronika E. Hubeny, Mukund Rangamani, and Erik Tonni, “Thermalization of Causal Holographic Information,” *JHEP* **05**, 136 (2013), arXiv:1302.0853 [hep-th].
- [25] Hong Liu and S. Josephine Suh, “Entanglement Tsunami: Universal Scaling in Holographic Thermalization,” *Phys. Rev. Lett.* **112**, 011601 (2014), arXiv:1305.7244 [hep-th].
- [26] Hong Liu and S. Josephine Suh, “Entanglement growth during thermalization in holographic systems,” *Phys. Rev. D* **89**, 066012 (2014), arXiv:1311.1200 [hep-th].
- [27] Mukund Rangamani, Moshe Rozali, and Alexandre Vincart-Emard, “Dynamics of Holographic Entanglement Entropy Following a Local Quench,” *JHEP* **04**, 069 (2016), arXiv:1512.03478 [hep-th].
- [28] Stefan Leichenauer and Mudassir Moosa, “Entanglement Tsunami in (1+1)-Dimensions,” *Phys. Rev. D* **92**, 126004 (2015), arXiv:1505.04225 [hep-th].
- [29] Pasquale Calabrese and John Cardy, “Quantum quenches in 1 + 1 dimensional conformal field theories,” *J. Stat. Mech.* **1606**, 064003 (2016), arXiv:1603.02889 [cond-mat.stat-mech].
- [30] Márk Mezei and Julio Virrueta, “The Quantum Null Energy Condition and Entanglement Entropy in Quenches,” (2019), arXiv:1909.00919 [hep-th].
- [31] Ofer Aharony, Steven S. Gubser, Juan Martin Maldacena, Hirosi Ooguri, and Yaron Oz, “Large N field theories, string theory and gravity,” *Phys. Rept.* **323**, 183–386 (2000), arXiv:hep-th/9905111.
- [32] J. David Brown and M. Henneaux, “Central Charges in the Canonical Realization of Asymptotic Symmetries: An Example from Three-Dimensional Gravity,” *Commun. Math. Phys.* **104**, 207–226 (1986).
- [33] M. Henningson and K. Skenderis, “The Holographic Weyl anomaly,” *JHEP* **07**, 023 (1998), arXiv:hep-th/9806087.
- [34] Vijay Balasubramanian and Per Kraus, “A Stress tensor for Anti-de Sitter gravity,” *Commun. Math. Phys.* **208**, 413–428 (1999), arXiv:hep-th/9902121.
- [35] Konstadinos Sfetsos, “On gravitational shock waves in curved space-times,” *Nucl. Phys. B* **436**, 721–745 (1995), arXiv:hep-th/9408169.
- [36] Maximo Banados, “Three-dimensional quantum geometry and black holes,” *AIP Conf. Proc.* **484**, 147–169 (1999), arXiv:hep-th/9901148.
- [37] G. Compère, Pujian Mao, A. Seraj, and M. M. Sheikh-Jabbari, “Symplectic and Killing symmetries of AdS₃ gravity: holographic vs boundary gravitons,” *JHEP* **01**, 080 (2016), arXiv:1511.06079 [hep-th].
- [38] M. M. Sheikh-Jabbari and H. Yavartanoo, “On 3d bulk geometry of Virasoro coadjoint orbits: orbit invariant charges and Virasoro hair on locally AdS₃ geometries,” *Eur. Phys. J. C* **76**, 493 (2016), arXiv:1603.05272 [hep-th].
- [39] Christian Ecker, Daniel Grumiller, Wilke van der Schee, M.M. Sheikh-Jabbari, and Philipp Stanzer, “Quantum Null Energy Condition and its (non)saturation in 2d CFTs,” *SciPost Phys.* **6**, 036 (2019), arXiv:1901.04499 [hep-th].
- [40] Maximo Banados, Claudio Teitelboim, and Jorge Zanelli, “The Black hole in three-dimensional space-time,” *Phys. Rev. Lett.* **69**, 1849–1851 (1992), arXiv:hep-th/9204099.
- [41] Maximo Banados, Marc Henneaux, Claudio Teitelboim, and Jorge Zanelli, “Geometry of the (2+1) black hole,” *Phys. Rev. D* **48**, 1506–1525 (1993), [Erratum: *Phys.Rev.D* **88**, 069902 (2013)], arXiv:gr-qc/9302012.
- [42] Stephen H. Shenker and Douglas Stanford, “Black holes and the butterfly effect,” *JHEP* **03**, 067 (2014), arXiv:1306.0622 [hep-th].
- [43] Shinsei Ryu and Tadashi Takayanagi, “Holographic derivation of entanglement entropy from AdS/CFT,”

- Phys. Rev. Lett. **96**, 181602 (2006), arXiv:hep-th/0603001.
- [44] Veronika E. Hubeny, Mukund Rangamani, and Tadashi Takayanagi, “A Covariant holographic entanglement entropy proposal,” JHEP **07**, 062 (2007), arXiv:0705.0016 [hep-th].
 - [45] Christoph Holzhey, Finn Larsen, and Frank Wilczek, “Geometric and renormalized entropy in conformal field theory,” Nucl. Phys. B **424**, 443–467 (1994), arXiv:hep-th/9403108.
 - [46] Mariano Cadoni and Maurizio Melis, “Holographic entanglement entropy of the BTZ black hole,” Found. Phys. **40**, 638–657 (2010), arXiv:0907.1559 [hep-th].
 - [47] M. M. Sheikh-Jabbari and H. Yavartanoo, “Excitation entanglement entropy in two dimensional conformal field theories,” Phys. Rev. D **94**, 126006 (2016), arXiv:1605.00341 [hep-th].
 - [48] Curtis T. Asplund, Alice Bernamonti, Federico Galli, and Thomas Hartman, “Entanglement Scrambling in 2d Conformal Field Theory,” JHEP **09**, 110 (2015), arXiv:1506.03772 [hep-th].
 - [49] Curt von Keyserlingk, Tibor Rakovszky, Frank Pollmann, and Shivaji Sondhi, “Operator hydrodynamics, OTOCs, and entanglement growth in systems without conservation laws,” Phys. Rev. X **8**, 021013 (2018), arXiv:1705.08910 [cond-mat.str-el].
 - [50] Márk Mezei and Douglas Stanford, “On entanglement spreading in chaotic systems,” JHEP **05**, 065 (2017), arXiv:1608.05101 [hep-th].
 - [51] Veronika E. Hubeny, Henry Maxfield, Mukund Rangamani, and Erik Tonni, “Holographic entanglement plateaux,” JHEP **08**, 092 (2013), arXiv:1306.4004 [hep-th].
 - [52] Jonah Kudler-Flam, “Relative Entropy of Random States and Black Holes,” Phys. Rev. Lett. **126**, 171603 (2021), arXiv:2102.05053 [hep-th].
 - [53] Jonah Kudler-Flam, Vladimir Narovlansky, and Shinsei Ryu, “Distinguishing Random and Black Hole Microstates,” (2021), arXiv:2108.00011 [hep-th].
 - [54] Gautam Mandal, Ritam Sinha, and Nilakash Sorokhaibam, “The inside outs of $\text{AdS}_3/\text{CFT}_2$: exact AdS wormholes with entangled CFT duals,” JHEP **01**, 036 (2015), arXiv:1405.6695 [hep-th].
 - [55] Johanna Erdmenger, Daniel Fernandez, Mario Flory, Eugenio Megias, Ann-Kathrin Straub, and Piotr Witkowski, “Time evolution of entanglement for holographic steady state formation,” JHEP **10**, 034 (2017), arXiv:1705.04696 [hep-th].
 - [56] Thomas Hartman and Juan Maldacena, “Time Evolution of Entanglement Entropy from Black Hole Interiors,” JHEP **05**, 014 (2013), arXiv:1303.1080 [hep-th].
 - [57] Horacio Casini, Eduardo Teste, and Gonzalo Torroba, “Modular Hamiltonians on the null plane and the Markov property of the vacuum state,” J. Phys. A **50**, 364001 (2017), arXiv:1703.10656 [hep-th].
 - [58] Avik Banerjee, Tanay Kibe, Nehal Mittal, Ayan Mukhopadhyay, and Pratik Roy, “to appear soon,” .
 - [59] Takahiro Sagawa, “Second law, entropy production, and reversibility in thermodynamics of information,” (2017), arXiv:1712.06858 [cond-mat.stat-mech].
 - [60] Massimiliano Esposito, Katja Lindenberg, and Christian Van den Broeck, “Entropy production as correlation between system and reservoir,” New Journal of Physics **12**, 013013 (2010).
 - [61] David Reeb and Michael M Wolf, “An improved landauer principle with finite-size corrections,” New Journal of Physics **16**, 103011 (2014).
 - [62] The geodesic distance between two end points (T_1, X_1, R_1) and (T_2, X_2, R_2) in the Poincaré patch metric given by (2) with $m(t, x) = j(t, x) = 0$ is simply $L \ln(\xi + \sqrt{\xi^2 - 1})$ where $\xi = (Z_1^2 + Z_2^2 - (T_1 + Z_1 - T_2 - Z_2)^2 + (X_1 - X_2)^2)/2Z_1Z_2$ with $Z_{1,2} = L^2/R_{1,2}$.
 - [63] Souvik Banerjee, Takaaki Ishii, Lata Kh Joshi, Ayan Mukhopadhyay, and P. Ramadevi, “Time-dependence of the holographic spectral function: Diverse routes to thermalisation,” JHEP **08**, 048 (2016), arXiv:1603.06935 [hep-th].